

THE 1% CONCORDANCE HUBBLE CONSTANT

C. L. BENNETT, D. LARSON, AND J. L. WEILAND

Johns Hopkins University and
3400 N. Charles St, Baltimore, MD 21218

AND

G. HINSHAW

Dept. of Physics and Astronomy, University of British Columbia and
Vancouver, BC Canada V6T 1Z1

Draft version October 14, 2014

ABSTRACT

The determination of the Hubble constant has been a central goal in observational astrophysics for nearly 100 years. Extraordinary progress has occurred in recent years on two fronts: the cosmic distance ladder measurements at low redshift and cosmic microwave background (CMB) measurements at high redshift. The CMB is used to predict the current expansion rate through a best-fit cosmological model. Complementary progress has been made with baryon acoustic oscillation (BAO) measurements at relatively low redshifts. While BAO data do not independently determine a Hubble constant, they are important for constraints on possible solutions and checks on cosmic consistency. A precise determination of the Hubble constant is of great value, but it is more important to compare the high and low redshift measurements to test our cosmological model. Significant tension would suggest either uncertainties not accounted for in the experimental estimates, or the discovery of new physics beyond the standard model of cosmology. In this paper we examine in detail the tension between the CMB, BAO, and cosmic distance ladder data sets. We find that these measurements are consistent within reasonable statistical expectations, and we combine them to determine a best-fit Hubble constant of $69.6 \pm 0.7 \text{ km s}^{-1} \text{ Mpc}^{-1}$. This value is based upon WMAP9+SPT+ACT+6dFGS+BOSS/DR11+ H_0 /Riess; we explore alternate data combinations in the text. The combined data constrain the Hubble constant to 1%, with no compelling evidence for new physics.

1. INTRODUCTION

Hubble's original attempt to establish the distance-redshift relation (Hubble 1929) highlighted the difficulty of establishing accurate distances over a sufficient volume of the universe while controlling systematic measurement errors. This lesson was reinforced in the decades-old debate between de Vaucouleurs and Sandage, who claimed Hubble constant values of ~ 100 and $\sim 50 \text{ km s}^{-1} \text{ Mpc}^{-1}$, respectively. In part, this debate motivated the *Hubble Space Telescope* (HST) and its Key Project to determine the Hubble constant, which produced $H_0 = 72 \pm 8 \text{ km s}^{-1} \text{ Mpc}^{-1}$ (Freedman et al. 2001). Efforts over the past dozen years have produced similar values, but the uncertainties have been reduced from $\sim 11\%$ to $\sim 3\%$: $73.8 \pm 2.4 \text{ km s}^{-1} \text{ Mpc}^{-1}$ (Riess et al. 2011); see also Freedman & Madore (2010, 2013) and Livio & Riess (2013) for more detailed reviews. Perhaps not surprisingly, the current measurements of H_0 lie near the mean of the de Vaucouleurs and Sandage values.

In recent years, Hubble constant measurements based on the cosmic distance ladder have been complemented by measurements using the cosmic microwave background (CMB). By determining the energy budget of the universe from the CMB power spectra (including polarization), the Friedmann equation determines the dynamics of the universe and hence the value of the Hubble constant through the cosmological model. The nine-year *Wilkinson Microwave Anisotropy Probe* (WMAP) data,

taken alone, but assuming a flat universe, give a 3% determination of $H_0 = 70.0 \pm 2.2 \text{ km s}^{-1} \text{ Mpc}^{-1}$ (Bennett et al. 2013; Hinshaw et al. 2013). When WMAP data are combined with smaller angular scale CMB data from the South Pole Telescope (SPT) and the Atacama Cosmology Telescope (ACT), and with distance measurements derived from baryon acoustic oscillation (BAO) observations in the range $0.1 < z < 0.6$, one obtains $H_0 = 68.76 \pm 0.84 \text{ km s}^{-1} \text{ Mpc}^{-1}$, a 1.2% determination. The *Planck* Collaboration (Planck XVI 2013) found a six-parameter flat Λ CDM model to be a good fit to their data and derived best-fit Hubble constant of $67.3 \pm 1.2 \text{ km s}^{-1} \text{ Mpc}^{-1}$. They note a $\approx 2.5\sigma$ tension with the Riess et al. (2011) cosmic distance ladder measurement.

Since the two approaches to measuring H_0 sample different epochs in cosmic history, this apparent tension has led to guarded speculation that new physics beyond the standard cosmological model may be needed to reconcile them (e.g., Wyman et al. 2014; Hamann & Hasenkamp 2013; Battye & Moss 2014; Dvorkin et al. 2014). However, as noted by others (e.g., Verde et al. 2014; Gao & Gong 2014; Efstathiou 2014), the tension could simply be the result of uncharacterized systematics in the individual H_0 determinations, or a statistical fluke, and these possibilities should be explored. In this paper, we re-examine the consistency of the H_0 measurements. In Section 2 we describe the recent relevant data; we present our analysis in Section 3; and we offer conclusions in Section 4.

2. DATA

We consider three primary data sets for establishing constraints on the Hubble constant: cosmic distance scale measurements, BAO measurements, and CMB measurements, and we describe each in turn.

2.1. Cosmic Distance Scale Measurements

Riess et al. (2011) found $H_0 = 73.8 \pm 2.4 \text{ km s}^{-1} \text{ Mpc}^{-1}$ including systematic uncertainties. Their result was based on three methods for finding distances to Type Ia supernovae and therefore calibrating their luminosities: (1) a geometric distance to NGC 4258 based on megamaser measurements, (2) parallax distances to 13 Milky Way Cepheids from *HST* and *Hipparcos* data, and (3) eclipsing binary distances to 92 collocated Cepheids in the Large Magellanic Cloud. Independently, Freedman et al. (2012) recalibrated the *HST* Key Project distance ladder using mid-infrared observations of Cepheids to minimize some of the systematic effects present in optical observations; they obtain $H_0 = 74.3 \pm 1.5$ (statistical) ± 2.1 (systematic). Both WMAP (Bennett et al. 2013; Hinshaw et al. 2013) and *Planck* (Planck XVI 2013) adopted the Riess et al. (2011) value for their 2013 analyses that included an H_0 prior.

Since the Riess et al. (2011) publication, there have been proposed revisions to the underlying distance calibration and/or to the selection of calibrators. Humphreys et al. (2013) recalibrated the geometric distance to NGC 4258 and used that distance to calibrate the Cepheids in NGC 4258. That work resulted in a value of $H_0 = 72.0 \pm 3.0 \text{ km s}^{-1} \text{ Mpc}^{-1}$ using only NGC 4258 as an anchor. Efstathiou (2014) makes a different Cepheid selection and uses the Humphreys et al. (2013) distance to NGC 4258 to obtain $H_0 = 70.6 \pm 3.3 \text{ km s}^{-1} \text{ Mpc}^{-1}$, using the NGC 4258 recalibration alone, and $H_0 = 72.5 \pm 2.5 \text{ km s}^{-1} \text{ Mpc}^{-1}$ using all three calibration methods. Riess (2014) combines the Humphreys recalibration with the other two calibration methods used in the original Riess et al. (2011) to obtain $H_0 = 73.0 \pm 2.4 \text{ km s}^{-1} \text{ Mpc}^{-1}$, making use of all available calibrator data and the original Riess et al. (2011) outlier cut methodology. For our analysis we adopt H_0 from Riess (2014).

2.2. Baryon Acoustic Oscillation Data

The remnants of BAOs in the early universe imprint a characteristic scale in the two-point correlation function of large scale structure. The BAO scale, r_s , is the distance a sound wave traveled in the baryon-photon plasma until decoupling at redshift z_d ; it is common to define $r_d \equiv r_s(z_d)$. Since the fluid is relativistic, the sound speed is well determined, so the BAO scale depends primarily on the age of the universe at decoupling, which depends only weakly on the cosmic matter and radiation densities (Reid et al. 2002).

BAO measurements do not, by themselves, constrain H_0 , but they are valuable for measuring relative distances as a function of redshift. The angular extent of the BAO scale at a given redshift determines the relative angular diameter distance, $D_A(z)/r_d$, while the radial extent, Δz , determines the Hubble parameter $H(z)$. It is convenient to define a volume-averaged effective distance,

$D_V \equiv (D_A^2 cz/H)^{1/3}$ (Eisenstein et al. 2005), and a fiducial value of the BAO scale, $r_{d,\text{fid}}$, for a fiducial cosmological model. One can then quote observational results as a distance, $D_V(z) \cdot (r_{d,\text{fid}}/r_d)$. The fiducial distance depends on cosmological parameters (such as H_0), however it is only used as a reference value and does not propagate into the BAO results that we analyze.

Table 1 summarizes the most recent BAO data for redshifts of 0.106, 0.32, 0.57 and 2.34. With the exception of the lowest redshift, these results are from the 11th Baryon Oscillation Sky Survey (BOSS) CMASS (“constant mass”) data release, DR11. There are several papers that analyze these data, and as noted in Beutler et al. (2014), they produce results within 1σ of each other. For the redshift 0.32 and 0.57 results, we adopt the “consensus” values from Anderson et al. (2014).

Currently, BAO results at higher redshift ($2.1 \leq z \leq 3.5$) come from the analysis of quasar Ly- α forest lines (Delubac et al. 2014; Font-Ribera et al. 2014), and are derived somewhat differently. Results are reported as separate radial and tangential determinations in the form $\alpha_{\parallel} \propto c/(H(z)r_d)$ and $\alpha_{\perp} \propto D_A(z)/r_d$, respectively. The radial measurement is substantially more precise than the tangential one. We “optimally combine” the radial and tangential Ly- α data as $\alpha_{\parallel}^{0.7} \alpha_{\perp}^{0.3}$ (Delubac et al. 2014). We obtain the value $\alpha_{\parallel}^{0.7} \alpha_{\perp}^{0.3} = 1.017 \pm 0.015$ from the combined contours of the cross- and auto-correlation likelihoods in Figure 13 of that paper, and we use this as our $z = 2.34$ likelihood.

2.3. Cosmic Microwave Background Data

2.3.1. WMAP

The WMAP9 data, when used without other measurements, gives a Hubble constant of $H_0 = 70.0 \pm 2.2 \text{ km s}^{-1} \text{ Mpc}^{-1}$ for a flat, six-parameter Λ CDM universe (Bennett et al. 2013; Hinshaw et al. 2013). Adding the ACT, SPT, and BAO data that were available as of mid-December 2012, the value drops somewhat to $H_0 = 68.76 \pm 0.84 \text{ km s}^{-1} \text{ Mpc}^{-1}$ (Hinshaw et al. 2013), independent of the cosmic distance scale measurements. Adding the Riess et al. (2011) H_0 prior of $73.8 \pm 2.4 \text{ km s}^{-1} \text{ Mpc}^{-1}$ to the WMAP9+ACT+SPT+BAO analysis gives $H_0 = 69.32 \pm 0.80 \text{ km s}^{-1} \text{ Mpc}^{-1}$ (Bennett et al. 2013; Hinshaw et al. 2013). We discuss combinations of WMAP9 with more recent data sets in Section 3.

2.3.2. Planck

The *Planck* Collaboration (Planck XVI 2013) gives a best-fit value of $67.3 \pm 1.2 \text{ km s}^{-1} \text{ Mpc}^{-1}$, derived from a six-parameter flat, Λ CDM model. Their analysis makes slightly different assumptions from those used by the WMAP team. The *Planck* collaboration assumed a total neutrino mass of $\sum m_{\nu} = 0.06 \text{ eV}$, corresponding to a physical neutrino density of $\Omega_{\nu} h^2 \approx 6 \times 10^{-4}$ (Planck XVI 2013). In addition, they vary the helium fraction, Y_{He} , as a function of both the physical baryon density, $\Omega_b h^2$, and the number of effective relativistic degrees of freedom in the early universe, N_{eff} , per the big bang nucleosynthesis (BBN) prediction, obtained by interpolating the PArthENoPE BBN code (Planck XVI 2013; Pisanti et al. 2008). Note that the Y_{He} fluctuations in a Markov chain have a standard deviation less than 0.1%

TABLE 1
BAO MEASUREMENTS

Quantity	z	Value	Experiment	Reference
$D_V \frac{r_d, \text{fid}}{r_d}$	0.106	457 ± 20 Mpc	6dFGS	Beutler et al. (2011) ^a
$D_V \frac{r_d, \text{fid}}{r_d}$	0.32	1264 ± 25 Mpc	BOSS DR11	Anderson et al. (2014) ^b
$D_V \frac{r_d, \text{fid}}{r_d}$	0.57	2056 ± 20 Mpc	BOSS DR11	Anderson et al. (2014)
D_A / r_d	2.34	10.93 ± 0.34	BOSS DR11	Delubac et al. (2014) ^c
$\frac{c}{H r_d}$	2.34	9.15 ± 0.20	BOSS DR11	Delubac et al. (2014) ^c

^a Beutler et al. (2011) quote their result in the form $r_d/D_V = 0.336 \pm 0.015$. This formulation assumes r_d follows the fitting formula of Eisenstein & Hu (1998) rather than the CAMB version discussed by Anderson et al. (2014). We quote their result in this form for consistency with the BOSS DR11 results.

^b Anderson et al. (2014) quote the $z = 0.32$ results from Tojeiro et al. (2014).

^c The Ly- α forest results do not optimally combine to a value for D_V , so we quote separate radial and tangential components, derived from a combination of auto- and cross-correlation statistics. As described in the text, we use an optimal combination of these values for our $z = 2.34$ likelihood.

of the mean Y_{He} value, for a simple Λ CDM model where $N_{\text{eff}} = 3.046$ is held constant. Allowing Y_{He} to vary in this fashion does not provide an extra degree of freedom, because Y_{He} is effectively constrained by $\Omega_b h^2$. If these BBN assumptions are applied to the WMAP9 data, the WMAP9-only Λ CDM value of H_0 is reduced by 0.3 to $69.7 \pm 2.2 \text{ km s}^{-1} \text{ Mpc}^{-1}$ (based on the WMAP9 chains released by the Planck collaboration).

The results noted above are from the Planck team’s first – and at this time only – cosmological data release of March 2013. In version 2 of Planck XVI (2013), dated December 2013, it is shown in Appendix C.4 that noise from a 4 K cooler line produces a systematic dip in the 217 GHz power spectrum around multipole $l = 1800$. When they marginalize over a spectrum template intended to mimic this cooler line, the value of the Hubble constant derived from the full data set increases by 0.3σ . There is no plan to formally update the publicly available Markov chains to include this effect until the next data release, and the inputs required to do so are not currently available (see also Spergel et al. (2013)), thus all Planck-based numbers in this paper are derived from the initially released data. Given this somewhat uncertain situation, our final estimate of H_0 uses WMAP9+ACT+SPT CMB data, which produces a conservative uncertainty.

2.3.3. ACT and SPT

Both WMAP and Planck use supplementary data at small angular scales from the two ground-based experiments, ACT and SPT. For Planck-based results, we use the publicly available Planck chains which incorporate ACT and SPT data available circa 2013. For WMAP-based results, we briefly quote results from the WMAP9 release (Bennett et al. 2013; Hinshaw et al. 2013), which incorporated ACT and SPT data available circa 2012; the new WMAP9-based results presented here incorporate the most recent ACT and SPT likelihoods.

The current ACT temperature and lensing likelihoods are discussed in Das et al. (2014) and Dunkley et al. (2013), while the most recent SPT likelihoods are discussed in Story et al. (2013) and van Engelen et al. (2012). A code that incorporates both ACT and SPT temperature likelihoods, called `actlite`, is described in Section 5 of Dunkley et al. (2013), and has been

made available on LAMBDA¹. We use this code in the mode where it uses the ACT-E(quatorial) and SPT data, ignoring the ACT-S(southern) field to avoid double-counting the overlapping SPT and ACT-S fields. We supplement the `actlite` likelihood with the lensing likelihoods described in Das et al. (2014) and van Engelen et al. (2012).

3. ANALYSIS

Our analysis proceeds in two steps: first, we form various weighted averages of the CMB, BAO, and distance ladder data sets to determine the overall best value of H_0 ; these results are summarized in Table 2. All CMB+BAO results in this table assume a flat, six-parameter Λ CDM cosmology. Then, we test whether the individual measurements are consistent with one another across techniques; we find that they are.

As noted in Section 2.3.2, the released WMAP9/2013 and Planck chains have different assumptions about massive neutrinos and helium. For the WMAP9-based results in Figures 1, 2, and 3, we have generated new Markov chains (denoted WMAP9/2014 in Table 2) with $\sum m_\nu = 0.06$ eV and the helium consistency relationship in Equation 8 of Sievers et al. (2013). Where noted, we include the most recent ACT and SPT data (Section 2.3.3). We adopt the March 2013 version of the Code for Anisotropies in the Microwave Background (CAMB)², which is the same version used by Planck.

The weighted average results are reported in Table 2. The format of the table is as follows: the data sets we employ are listed in the first column; where that data set sufficiently constrains H_0 by itself, we quote that value in the second column. Subsequent columns, labeled A through H, indicate different combinations of data, and their weighted average is given in the bottom row of each column. Columns A and B contain Planck-based data sets (Planck XVI 2013), both without (Column A) and re-weighted with (Column B) the local H_0 value included. Column C gives the WMAP9+ACT+SPT+BAO result reported by Hinshaw et al. (2013), with no H_0 prior. Column D adds an H_0

¹ <http://lambda.gsfc.nasa.gov/product/act/act.cmblikelihood.get.cfm>, version 2.2

² <http://camb.info>

TABLE 2
ESTIMATES OF THE HUBBLE CONSTANT FROM COMBINED DATA, ASSUMING Λ CDM

Data set	Combined results								
	H_0 km s ⁻¹ Mpc ⁻¹	A	B	C	D	E	F	G	H ^a
WMAP9/2013 ^b	70.0 ± 2.2			✓	✓	✓			
WMAP9/2014 ^c	69.4 ± 2.2						✓	✓	✓
Planck+WMAPPol/2013 ^d	67.3 ± 1.2	✓	✓						
ACT+SPT/2012 ^e	–			✓	✓	✓			
ACT+SPT/2013 ^e	–	✓	✓						
ACT+SPT/2014 ^e	–							✓	✓
BAO/2012 ^f	–			✓	✓	✓			
BAO/2013 ^f	–	✓	✓						
BAO/2014 ^f	–						✓	✓	✓
H_0 , Riess et al. (2011)	73.8 ± 2.4				✓				
H_0 , Riess (2014)	73.0 ± 2.4		✓			✓	✓		✓
Combined H_0 (km s ⁻¹ Mpc ⁻¹)		67.8	68.3	68.8	69.3	69.2	69.3	69.3	69.6
Combined σ (km s ⁻¹ Mpc ⁻¹)		0.8	0.7	0.8	0.8	0.8	0.8	0.7	0.7

^a Column H represents our current best-estimate concordance value of H_0 , 69.6 ± 0.7 km s⁻¹Mpc⁻¹, assuming flat Λ CDM.

^b WMAP9/2013: From Hinshaw et al. (2013). Assumes flat Λ CDM, with $\sum m_\nu = 0$, $Y_{\text{He}} = 0.24$, $N_{\text{eff}} = 3.04$ (instead of 3.046), and the January 2012 version of CAMB.

^c WMAP9/2014: This paper. Assumes flat Λ CDM, with $\sum m_\nu = 0.06$ eV, Y_{He} co-varies with $\Omega_b h^2$ per BBN, $N_{\text{eff}} = 3.046$, and the March 2013 version of CAMB.

^d Planck: From Planck XVI (2013). Assumes flat Λ CDM. Likelihood ($2 \leq l \leq 2500$)+lensing+low- l pixel-space polarization from the WMAP9 likelihood.

^e ACT+SPT/2012: Uses ACT and SPT data that were available as of the final WMAP9 release. ACT+SPT/2013: Uses data that were available as of the initial Planck release. ACT+SPT/2014: Uses data currently available for use in this paper.

^f BAO/2012: From Table 1 of Hinshaw et al. (2013). BAO/2013: From Section 5.2 of Planck XVI (2013). BAO/2014: From Table 1 of this paper.

prior, as reported by Bennett et al. (2013), and Column E gives the corresponding result re-weighted with the revised H_0 value in Riess (2014). Column F gives our new result based on (WMAP9+BAO+ H_0)/2014. Column G is the same as Column F, with the addition of ACT and SPT data, and the removal of the local H_0 prior. Column H is the same as Column F, with the addition of ACT and SPT data. As discussed below, Column H represents our current best-estimate concordance value of H_0 , 69.6 ± 0.7 km s⁻¹Mpc⁻¹.

We test consistency of the data in Figure 1. To compare H_0 , BAO, and CMB measurements, we present constraints in the space $\{H_0, D_V r_{d,\text{fid}}/r_d\}$ since this allows us to place H_0 measurements on the horizontal axis and BAO measurements orthogonally on the vertical axis. Since the $z = 0.57$ BAO measurements have the smallest errors (representing a 1% measurement of the distance scale), and since the other BAO measurements are largely consistent with the $z = 0.57$ measurement, we confine our plotted consistency checks to this BAO redshift only. We add CMB data by projecting the Monte Carlo Markov Chain points into this space.

Figure 1 contains three panels with CMB constraints derived assuming Λ CDM. The top panel shows WMAP9/2014 constraints, the middle panel shows (WMAP9+ACT+SPT)/2014, and the bottom panel shows (Planck+ACT+SPT)/2013, on the same scale for ease of comparison. To quantitatively assess consistency, we fit a 10-component two-dimensional (2D) Gaussian mixture function to the CMB chain points. This function is evaluated numerically on a large 2D grid and contours that enclose 68.27% and 95.45% of the probability are computed and plotted. (The accuracy of the Gaussian mixture can be checked by eye in Figures 1, 2, and 3,

where we plot the fitted contours over the chain points). The Gaussian mixture provides an analytic 2D likelihood which we can combine with the 2D BAO+ H_0 Gaussian likelihood (see below) to evaluate the best 2D fit.

We note that neither the BAO nor the local Hubble constant measurements have extra variables in their likelihoods that are correlated with CMB measurements in other dimensions. For example, neither the BAO measurement $D_V r_{d,\text{fid}}/r_d$ nor the local H_0 measurement depend on $\Omega_b h^2$, the scalar spectral index n_s , etc. While it is true that $r_d = r_s(z_d)$ does depend on $\Omega_b h^2$, the quantity measured by the BAO, $D_V r_{d,\text{fid}}/r_d$, is independent of r_d . Given this lack of correlated hidden variables, we can determine the consistency of these likelihoods directly in this 2D space.

Since the BAO and H_0 data each constrain one dimension of our parameter space, we can combine them into a single likelihood to get a 2D Gaussian likelihood that constrains both $D_V r_{d,\text{fid}}/r_d$ and H_0 . We take $H_0 = 73.0 \pm 2.4$ km s⁻¹Mpc⁻¹ (Riess 2014) and $D_V r_{d,\text{fid}}/r_d = 2056 \pm 20$ Mpc at $z = 0.57$ (Anderson et al. 2014) and plot the combined likelihood as grey ellipses in Figures 1, 2, and 3. We further note that the CMB likelihood for flat Λ CDM is well approximated by a single Gaussian in this space, producing contours that are virtually indistinguishable in Figure 1. Under the assumption that both experiments are measuring the same cosmological quantities with different noise, the covariance matrix of the difference between the two measurements is the sum of their individual covariance matrices.

For the WMAP9/2014 data in the top panel of Figure 1, we find the mean value of H_0 for the CMB-only likelihood to be 69.4 km s⁻¹Mpc⁻¹. The WMAP/2014

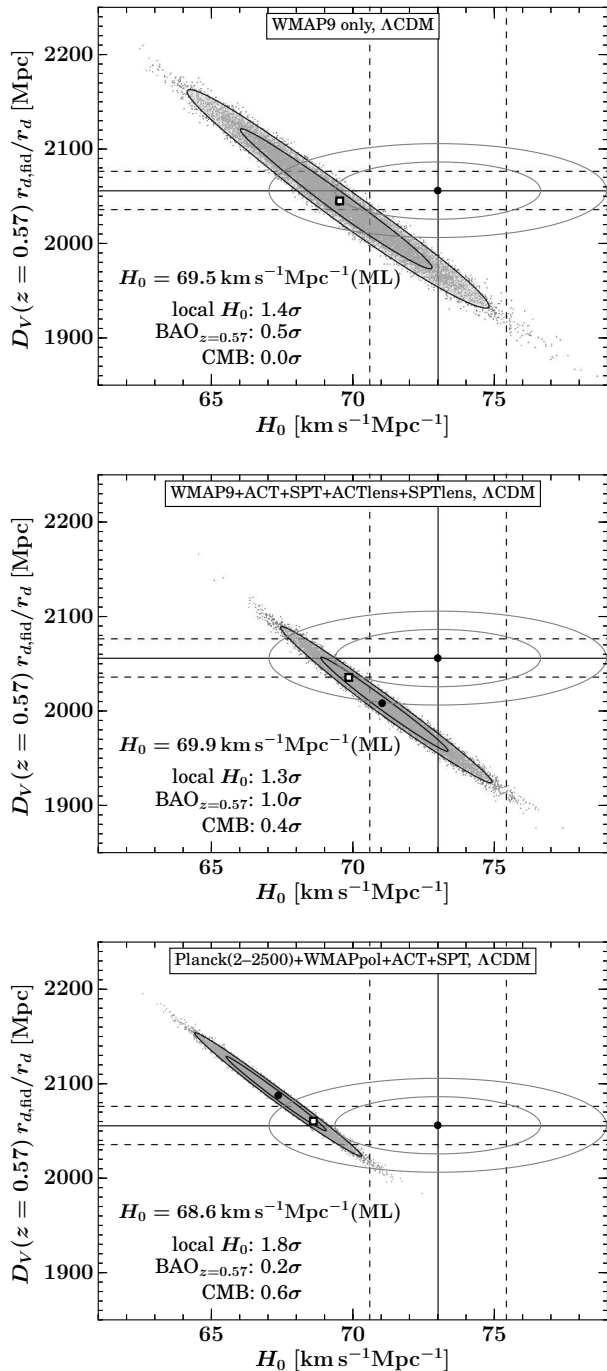


FIG. 1.— WMAP9-based (top, middle) and *Planck*-based (bottom) CMB data sets for a flat ΛCDM cosmological model, compared to local H_0 measurements and BAO data at $z = 0.57$. Gray points in the top panel are from this paper’s WMAP9/2014 chain; those in the middle panel are from (WMAP9+ACT+SPT)/2014. Gray points in the bottom panel are from the *Planck* chains (Planck XVI 2013) which include the (ACT+SPT)/2013 data combination (see text and Table 2). The peak of each 2D-marginalized CMB likelihood is indicated with a black filled circle and the contours for the chain points enclose 68% and 95% of the probability, as computed from a 10-component 2D Gaussian mixture fit (see text). The BAO and H_0 measurements are indicated by vertical and horizontal lines, respectively, with dashed lines showing 1σ error bars. The gray ellipses show 68% and 95% contours for the product of the BAO and H_0 likelihoods. The peak of the combined CMB+BAO+ H_0 likelihoods is indicated with an open square, and its value is noted in each panel.

H_0 and D_V values are entirely consistent with the BAO+ H_0 likelihood; the difference has a χ^2 of 2.5 for 2 degrees of freedom, with a probability to exceed (PTE) of 28%. Combining the three data sets gives a weighted mean of $H_0 = 69.5 \text{ km s}^{-1}\text{Mpc}^{-1}$, which is also clearly consistent with the individual data sets. The maxima of the separate CMB and H_0 +BAO likelihoods in this space are indicated with black filled circles, and the best fit to both distributions is indicated with an open square. The best fit H_0 value for the CMB, local H_0 , and $\text{BAO}_{z=0.57}$ likelihoods is also given in the figure. Because the more sophisticated Gaussian mixture fit changes the results only very slightly, we consider the single Gaussian approximation to be acceptable for checking consistency of the fit.

Using an identical analysis for the (WMAP9+ACT+SPT)/2014 data, we find the mean of the CMB-only likelihood to be $71.1 \text{ km s}^{-1}\text{Mpc}^{-1}$, with a χ^2 for the difference of 3.8, with a PTE of 15%. For the combined CMB+ H_0 +BAO $_{z=0.57}$ data, we find $H_0 = 69.8 \text{ km s}^{-1}\text{Mpc}^{-1}$. Again, this is quite close to the Gaussian mixture result in the middle panel of Figure 1.

For the *Planck*-based CMB data in the bottom panel of Figure 1, we find the mean value of H_0 for the CMB-only likelihood to be $67.3 \text{ km s}^{-1}\text{Mpc}^{-1}$. This is only slightly less consistent with the BAO+ H_0 likelihood; the difference has a χ^2 of 4.6 for 2 degrees of freedom and a PTE of 10%. The weighted mean of CMB+ H_0 +BAO $_{z=0.57}$ is $68.6 \text{ km s}^{-1}\text{Mpc}^{-1}$. This is 1.8σ from the central value of the local Hubble prior, and so is not significantly different.

As a further consistency check of the results in Figure 1, we list the deviations of the best fit point from each of the three likelihoods used (CMB, BAO $_{z=0.57}$, and H_0). The deviation is given in number of standard deviations, which is directly computable for the H_0 and BAO data. For the CMB, we compute the probability of the CMB Gaussian mixture likelihood to exceed the likelihood at the best fit point, and convert that into a number of standard deviations. None of these values are above 2σ , so the combined parameters are consistent with each individual likelihood.

As shown in Figure 1, both *Planck* and WMAP data fall along the same degeneracy line. This is primarily because they provide consistent measurements of the angular scale of the CMB peaks (see Page et al. (2003); Percival et al. (2002) for a discussion of these angular scales). The *Planck* result itself prefers a slightly lower H_0 values than WMAP, but when combined with BAO data we see that the BAO tends to pull *Planck* upward and WMAP downward, yielding closer agreement between combined H_0 values for CMB+BAO+ H_0 results. Therefore, it does not matter greatly whether we use the WMAP9+ACT+SPT or *Planck*+ACT+SPT data combination since they both constrain the ultimate H_0 fit value by virtue of following the same CMB degeneracy line. Since the *Planck* team has only had one data release so far and has not yet released revised chains reflecting the correction for the 4 K cooler line effect mentioned in Section 2.3.2, we consider WMAP9+ACT+SPT CMB data in the remainder of this analysis. We look forward to future releases of *Planck* data, and in particular the

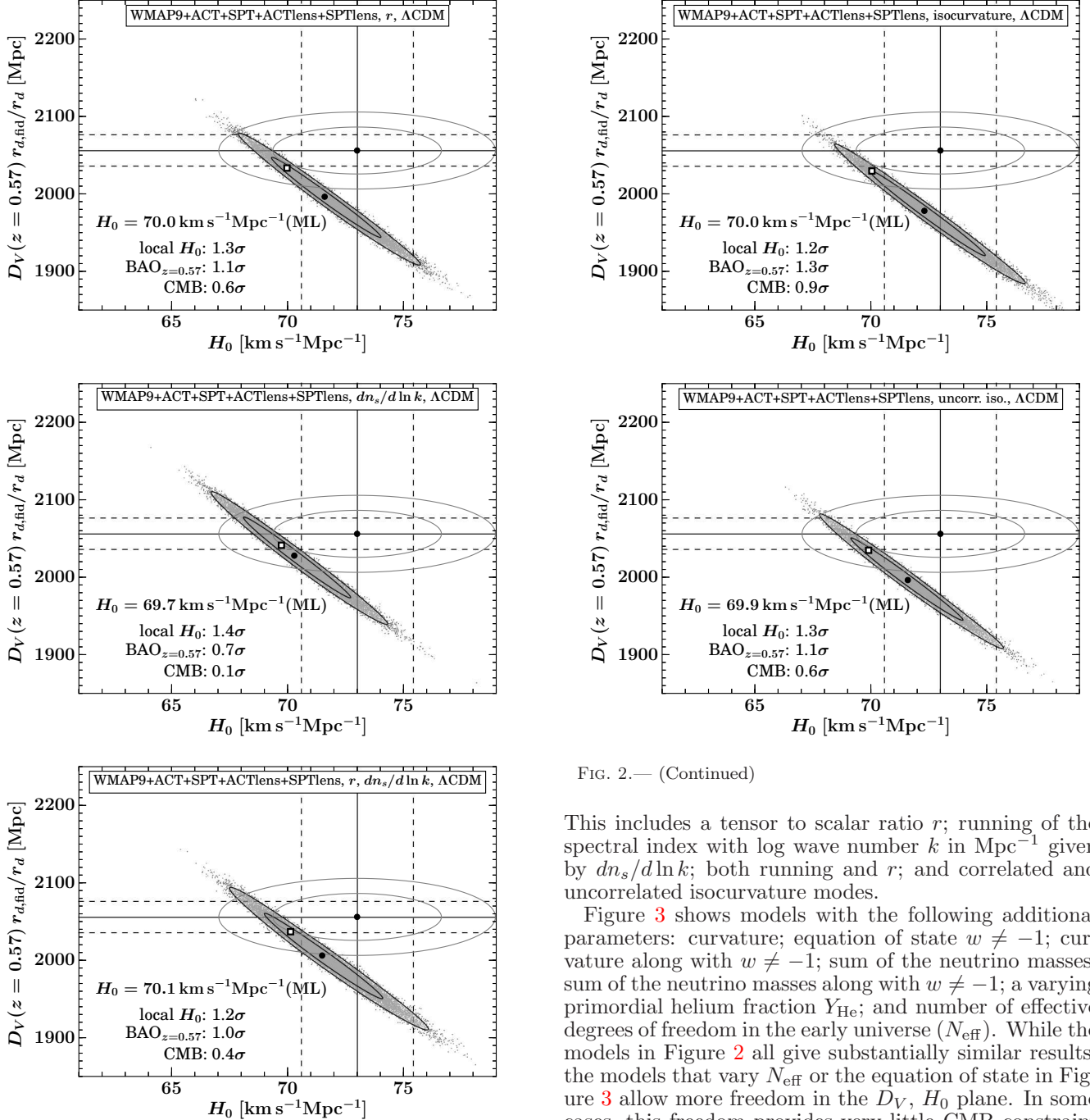


FIG. 2.— Combination of $z = 0.57$ BAO, local H_0 , and CMB data. Gray points and contours are from (WMAP9+ACT+SPT)/2014, as described in the text. The black filled circle is the peak of the 2D marginalized CMB likelihood. The concordance value, the open square, is maximum likelihood of the product of the 2D CMB, BAO, and H_0 likelihoods.

updated chains and accompanying likelihood which will permit further independent analyses.

In Figures 2 and 3 we plot constraints on H_0 and a BAO-measured distance to $z = 0.57$ for various cosmological models, to investigate the dependence on model. We find that the constraint from the CMB on all the models in Figure 2 is largely the same; all these models predict the same expansion history of the universe.

FIG. 2.— (Continued)

This includes a tensor to scalar ratio r ; running of the spectral index with log wave number k in Mpc^{-1} given by $dn_s/d \ln k$; both running and r ; and correlated and uncorrelated isocurvature modes.

Figure 3 shows models with the following additional parameters: curvature; equation of state $w \neq -1$; curvature along with $w \neq -1$; sum of the neutrino masses; sum of the neutrino masses along with $w \neq -1$; a varying primordial helium fraction Y_{He} ; and number of effective degrees of freedom in the early universe (N_{eff}). While the models in Figure 2 all give substantially similar results, the models that vary N_{eff} or the equation of state in Figure 3 allow more freedom in the D_V, H_0 plane. In some cases, this freedom provides very little CMB constraint at all, thus allowing BAO+ H_0 to dominate the combined result. In the case of the w CDM plot with massive neutrinos, all that can really be concluded is that the CMB likelihood is relatively flat over the BAO and H_0 best fit region, and still consistent with the WMAP9 cosmological priors.

In practice, WMAP and Planck chains that include BAO data (such as those presented in Table 2) utilize BAO measurements over a range of redshifts. None of the currently released chains have included BAO data for $z > 1$. Representative BAO measurements at various redshifts (see Table 1) are plotted in Figure 4, for comparison purposes. Because these data mostly constrain the expansion history, we plot these as constraints on Ω_m

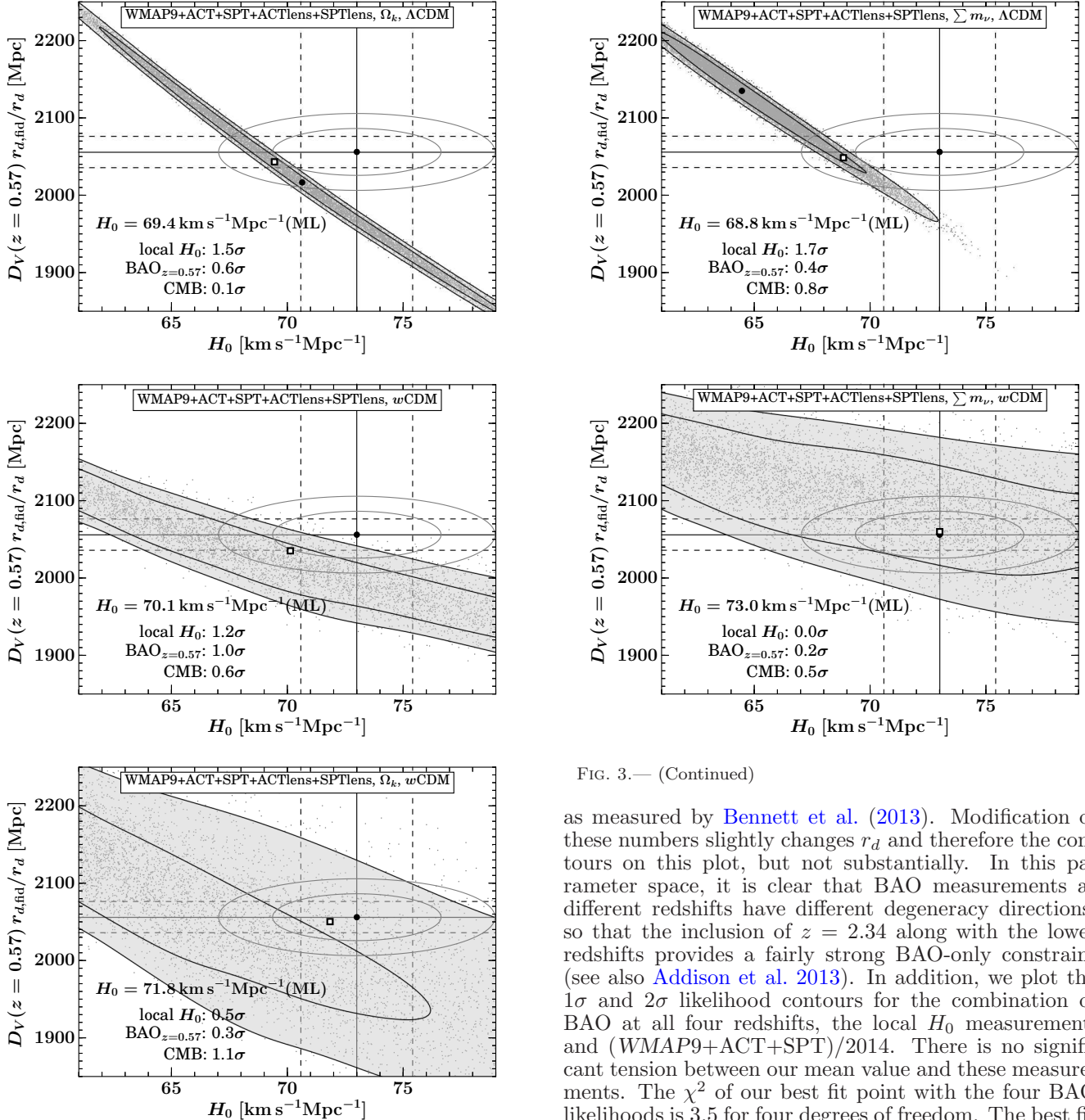


FIG. 3.— Combination of $z = 0.57$ BAO, H_0 , and CMB data, as in Figure 2, but now with additional cosmological parameters not required by the data such as space curvature and/or an equation of state parameter $w \neq -1$, and/or massive neutrinos. For models only weakly constrained by CMB data the 2D Gaussian mixture approach used is not ideal so the contours should be viewed with caution.

and H_0 . If we assume zero curvature, then $\Omega_m + \Omega_\Lambda = 1$ (neglecting tiny amounts of radiation and neutrinos), and so Ω_m and H_0 determine nearly the entire expansion history of the universe, and certainly the region measured by BAO. To obtain the drag radius that is directly measured by BAO, we assume the standard effective number of neutrinos ($N_{\text{eff}} = 3.046$), and set $\Omega_b h^2 = 0.02223$

FIG. 3.— (Continued)

as measured by Bennett et al. (2013). Modification of these numbers slightly changes r_d and therefore the contours on this plot, but not substantially. In this parameter space, it is clear that BAO measurements at different redshifts have different degeneracy directions, so that the inclusion of $z = 2.34$ along with the lower redshifts provides a fairly strong BAO-only constraint (see also Addison et al. 2013). In addition, we plot the 1σ and 2σ likelihood contours for the combination of BAO at all four redshifts, the local H_0 measurement, and (WMAP9+ACT+SPT)/2014. There is no significant tension between our mean value and these measurements. The χ^2 of our best fit point with the four BAO likelihoods is 3.5 for four degrees of freedom. The best fit $H_0 = 69.6 \pm 0.7$ km s⁻¹ Mpc⁻¹ is 1.4σ away from the local H_0 measurement. Finally, the best fit point is within the 1σ contour of the CMB points in this projection, so it is also a good fit to the CMB data.

4. CONCLUSIONS

1) Our combined dataset with CMB, BAO and distance ladder H_0 determinations results in a best-estimate concordance Hubble constant value of 69.6 ± 0.7 km s⁻¹ Mpc⁻¹. Given the currently available data, we argue that there is no compelling need for physics beyond standard flat Λ CDM to establish consistency between the H_0 values derived using three separate but complementary methods.

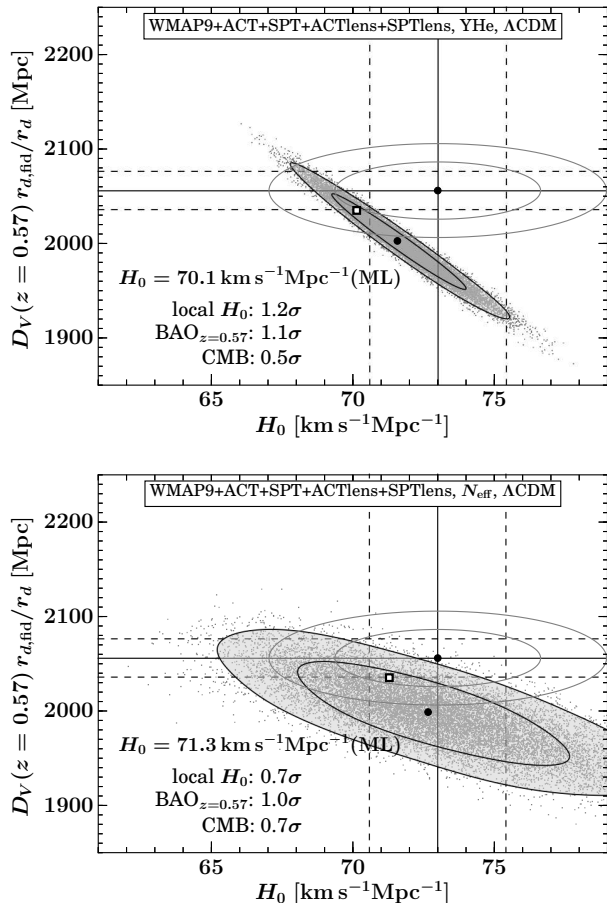


FIG. 3.— (Continued)

2) Following a similar analysis, the concordance value of $\Omega_m = 0.286 \pm 0.008$.

3) The previous $\approx 2.5\sigma$ tension between the H_0 values determined by [Planck XVI \(2013\)](#) and [Riess et al. \(2011\)](#) has been recently mitigated somewhat (to $< 2\sigma$) by a decrease in the distance ladder value by roughly 0.3σ ([Riess \(2014\)](#), based on a recalibrated megamaser distance) and a slight increase (also by $\approx 0.3\sigma$) in the *Planck* value derived assuming Λ CDM after correction for a 4 K cooler line instrumental effect ([Planck XVI 2013, Appendix C.4](#)). Since the data incorporating the cooling line correction are not yet public, we eagerly await the further insight into the Hubble constant that will become available with the next *Planck* data release.

4) Within the 2D D_V versus H_0 parameter space, CMB constraints tend to be confined along a thin diagonal which is defined primarily by the acoustic scale of the CMB power spectrum. As shown in Figure 1, both *Planck* and *WMAP* data provide very consistent measurements of the angular scale of the CMB peaks. *Planck* data occupy a slightly different location along the degeneracy line than do *WMAP* data. While the *Planck* result prefers a lower H_0 value than *WMAP*, the BAO results pull *Planck* upward and *WMAP* downward, yielding CMB+BAO+ H_0 results that differ by roughly $1 \text{ km s}^{-1} \text{ Mpc}^{-1}$. If the *Planck* solution for H_0 in the next formal parameter release is significantly lower than the *WMAP9*+*ACT*+*SPT* value, this would primarily indi-

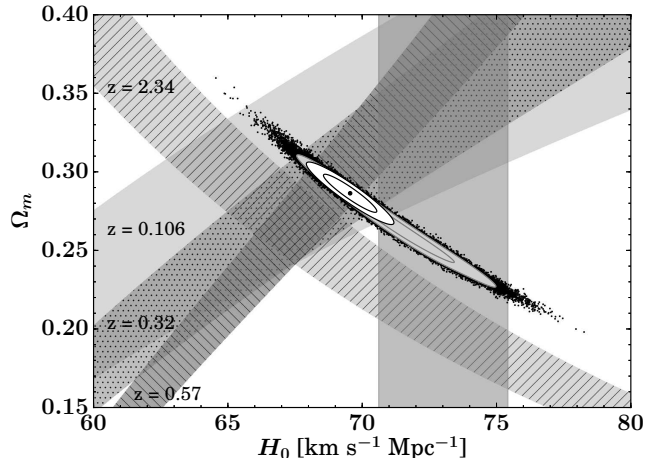


FIG. 4.— BAO 1σ constraints for redshifts 0.106 (r_s/D_V in [Beutler et al. 2011](#)), 0.32 and 0.57 ($D_V r_{d, \text{fid}}/r_d$ in [Anderson et al. 2014](#)), and 2.34 ($\alpha_{\parallel}^{0.7} \alpha_{\perp}^{0.3}$ in [Delubac et al. 2014](#)). For these contours, the value of $r_d = r_s(z_d)$ is computed using [Eisenstein & Hu \(1998\)](#) and corrected by a factor of 1.026 when comparing to r_d values computed using CAMB (everything except $z = 0.106$). The baryon density is assumed to be $\Omega_b h^2 = 0.02223$ ([Bennett et al. 2013](#)); changes of this value within the error bars do not substantially shift r_d and therefore the BAO contours. The black points are from the (*WMAP9*+*ACT*+*SPT*)/2014 Λ CDM Markov chain, with 1 and 2σ contours overlaid in gray. The H_0 value with 1σ uncertainty from [Riess \(2014\)](#) is indicated with the vertical shaded stripe. For our previous figures, we only use the $z = 0.57$ data set, since it is consistent with the other BAO data and has the smallest error bars. The combination of all likelihoods shown is given by the white 1σ and 2σ ellipses in the center of the figure. Marginalizing over the other cosmological parameters, we find $\Omega_m = 0.286 \pm 0.008$ for all likelihoods shown.

cate tension among the CMB data sets, which would require resolution before concluding that evidence for new physics is present.

5) We have shown that additional parameters are not necessary to have consistency among the CMB, BAO, and H_0 results. Should future measurements substantially increase the tension, this could be resolved with additional model parameters. Figure 3 shows that this is most easily done with additional relativistic degrees of freedom in the early universe (N_{eff}), or an equation of state not equal to -1 , but we again emphasize that current data do not require nonstandard values for these parameters.

6) It is vital to continue to improve the various measurements of H_0 in order to search for new physics. Of particular interest at this time would be a local H_0 determination with a precision smaller than that of our concordance value uncertainty. Of further clear interest are decreased uncertainties in the high redshift ($z > 2$) BAO determinations. We also recognize that there are always newer data coming on-line (e.g., Sloan Digital Sky Survey with larger survey volume, *Gaia* and WFC3 spatial scanning parallax results for better calibrator distances) and look forward to new contributions and constraints that these may provide.

We thank Adam Riess for useful comments. We also thank Daniel Eisenstein for suggesting the use of a Gaussian mixture model to fit the Markov chain points, and an anonymous referee for suggesting helpful clarifica-

tions. We acknowledge use of the `Scikit-learn`³ code (Pedregosa et al. 2011) for testing Gaussian mixture models. This research was supported in part by NASA grant NNX14AF64G and by the Canadian Institute for Advanced Research (CIFAR). We acknowledge use of the HEALPix (Gorski et al. 2005) and CAMB (Lewis

et al. 2000) packages. This research has made use of NASA’s Astrophysics Data System Bibliographic Services. We acknowledge the use of the Legacy Archive for Microwave Background Data Analysis (LAMBDA). Support for LAMBDA is provided by NASA Headquarters.

REFERENCES

- Addison, G. E., Hinshaw, G., & Halpern, M. 2013, *MNRAS*, 436, 1674, [1304.6984](#) [3]
- Anderson, L., Aubourg, É., Bailey, S., Beutler, F., Bhardwaj, V., et al. 2014, *MNRAS*, 441, 24, [1312.4877](#) [2.2, 1, 3, 4]
- Battye, R. A. & Moss, A. 2014, *Physical Review Letters*, 112, 051303, [1308.5870](#) [1]
- Bennett, C. L., Larson, D., Weiland, J. L., Jarosik, N., Hinshaw, G., et al. 2013, *ApJS*, 208, 20, [1212.5225](#) [1, 2.1, 2.3.1, 2.3.3, 3, 4]
- Beutler, F., Blake, C., Colless, M., Jones, D. H., Staveley-Smith, L., et al. 2011, *MNRAS*, 416, 3017, [1106.3366](#) [1, 4]
- Beutler, F., Saito, S., Seo, H.-J., Brinkmann, J., Dawson, K. S., et al. 2014, *MNRAS*, 443, 1065, [1312.4611](#) [2.2]
- Das, S., Louis, T., Nolta, M. R., Addison, G. E., Battistelli, E. S., et al. 2014, *J. Cosmology Astropart. Phys.*, 4, 014, [1301.1037](#) [2.3.3]
- Delubac, T., Bautista, J. E., Busca, N. G., Rich, J., Kirkby, D., et al. 2014, *ArXiv e-prints*, [1404.1801](#) [2.2, 1, 4]
- Dunkley, J., Calabrese, E., Sievers, J., Addison, G. E., Battaglia, N., et al. 2013, *J. Cosmology Astropart. Phys.*, 7, 025, [1301.0776](#) [2.3.3]
- Dvorkin, C., Wyman, M., Rudd, D. H., & Hu, W. 2014, *Phys. Rev. D*, 90, 083503, [1403.8049](#) [1]
- Efstathiou, G. 2014, *MNRAS*, [1311.3461](#) [1, 2.1]
- Eisenstein, D. J. & Hu, W. 1998, *ApJ*, 496, 605, [astro-ph/9709112](#) [1, 4]
- Eisenstein, D. J., Zehavi, I., Hogg, D. W., Scoccamarro, R., Blanton, M. R., et al. 2005, *ApJ*, 633, 560 [2.2]
- Font-Ribera, A., Kirkby, D., Busca, N., Miralda-Escudé, J., Ross, N. P., et al. 2014, *J. Cosmology Astropart. Phys.*, 5, 027, [1311.1767](#) [2.2]
- Freedman, W. L. & Madore, B. F. 2010, *ARA&A*, 48, 673, [1004.1856](#) [1]
- . 2013, *The Distance Scale of the Universe*, 423 [1]
- Freedman, W. L., Madore, B. F., Gibson, B. K., Ferrarese, L., Kelson, D. D., et al. 2001, *ApJ*, 553, 47 [1]
- Freedman, W. L., Madore, B. F., Scowcroft, V., Burns, C., Monson, A., et al. 2012, *ApJ*, 758, 24, [1208.3281](#) [2.1]
- Gao, Q. & Gong, Y. 2014, *Classical and Quantum Gravity*, 31, 105007, [1308.5627](#) [1]
- Gorski, K. M., Hivon, E., Banday, A. J., Wandelt, B. D., Hansen, F. K., et al. 2005, *ApJ*, 622, 759, [astro-ph/0409513](#) [4]
- Hamann, J. & Hasenkamp, J. 2013, *J. Cosmology Astropart. Phys.*, 10, 044, [1308.3255](#) [1]
- Hinshaw, G., Larson, D., Komatsu, E., Spergel, D. N., Bennett, C. L., et al. 2013, *ApJS*, 208, 19, [1212.5226](#) [1, 2.1, 2.3.1, 2.3.3, 2, 3]
- Hubble, E. 1929, *Proceedings of the National Academy of Science*, 15, 168 [1]
- Humphreys, E. M. L., Reid, M. J., Moran, J. M., Greenhill, L. J., & Argon, A. L. 2013, *ApJ*, 775, 13 [2.1]
- Lewis, A., Challinor, A., & Lasenby, A. 2000, *ApJ*, 538, 473 [4]
- Livio, M. & Riess, A. G. 2013, *Physics Today*, 66, 100000 [1]
- Page, L., Nolta, M. R., Barnes, C., Bennett, C. L., Halpern, M., et al. 2003, *ApJS*, 148, 233 [3]
- Pedregosa, F., Varoquaux, G., Gramfort, A., Michel, V., Thirion, B., et al. 2011, *Journal of Machine Learning Research*, 12, 2825 [4]
- Percival, W. J., Sutherland, W., Peacock, J. A., Baugh, C. M., Bland-Hawthorn, J., et al. 2002, *MNRAS*, 337, 1068 [3]
- Pisanti, O., Cirillo, A., Esposito, S., Iocco, F., Mangano, G., et al. 2008, *Computer Physics Communications*, 178, 956, [0705.0290](#) [2.3.2]
- Planck XVI, Ade, P. A. R., Aghanim, N., Armitage-Caplan, C., Arnaud, M., et al. 2013, *ArXiv e-prints*, [1303.5076](#) [1, 2.1, 2.3.2, 3, 2, 1, 4]
- Reid, D. D., Kittell, D. W., Arsznov, E. E., & Thompson, G. B. 2002, *ArXiv Astrophysics e-prints*, [astro-ph/0209504](#) [2.2]
- Riess, A. G. 2014, *Local Results*, Presented in the 2014 Cosmic Distance Scale Workshop, <http://www.stsci.edu/institute/conference/cosmic-distance/http://realserver4v.stsci.edu/t/data/2014/03/3951/AdamRiess033114.mp4> [2.1, 2, 3, 3, 4, 4]
- Riess, A. G., Macri, L., Casertano, S., Lampeitl, H., Ferguson, H. C., et al. 2011, *ApJ*, 730, 119, [1103.2976](#) [1, 2.1, 2.3.1, 2, 4]
- Sievers, J. L., Hlozek, R. A., Nolta, M. R., Acquaviva, V., Addison, G. E., et al. 2013, *J. Cosmology Astropart. Phys.*, 10, 060, [1301.0824](#) [3]
- Spergel, D., Flauger, R., & Hlozek, R. 2013, *ArXiv e-prints*, [1312.3313](#) [2.3.2]
- Story, K. T., Reichardt, C. L., Hou, Z., Keisler, R., Aird, K. A., et al. 2013, *ApJ*, 779, 86, [1210.7231](#) [2.3.3]
- Tojeiro, R., Ross, A. J., Burden, A., Samushia, L., Manera, M., et al. 2014, *MNRAS*, 440, 2222, [1401.1768](#) [1]
- van Engelen, A., Keisler, R., Zahn, O., Aird, K. A., Benson, B. A., et al. 2012, *ApJ*, 756, 142, [1202.0546](#) [2.3.3]
- Verde, L., Protopapas, P., & Jimenez, R. 2014, *ArXiv e-prints*, [1403.2181](#) [1]
- Wyman, M., Rudd, D. H., Vanderveld, R. A., & Hu, W. 2014, *Physical Review Letters*, 112, 051302 [1]

³ <http://scikit-learn.org/stable/index.html>